Publications of the Astronomical Society of the Pacific, 135:074202 (9pp), 2023 July https://doi.org/10.1088/1538-3873/ace3f5

A Study of Twelve Potential Merger Candidate Contact Binary Systems

Surjit S. Wadhwa[1], Bojan Arbutina[2], Nick F. H. Tothill[1], Miroslav D. Filipović[1], Ain Y. De Horta[1], Jelena Petrović[3], and Gojko Djurašević[3]

[1] School of Science, Western Sydney University, Locked Bag 1797, Penrith, NSW 2751, Australia; 19899347@student.westernsydney.edu.au
[2] Department of Astronomy, Faculty of Mathematics, University of Belgrade, Studentski trg 16, 11000 Belgrade, Serbia
[3] Astronomical Observatory, Volgina 7, 11060 Belgrade, Serbia
Received 2023 March 10; accepted 2023 July 4; published 2023 July 20

Abstract

Photometric observations and analysis of twelve previously poorly studied contact binary systems is presented. All show total eclipses and have extremely low mass ratios ranging from 0.072 to 0.15. Also, all show characteristics of orbital instability with mass ratios within the theoretical orbital instability range. Although none demonstrate a significant O'Connell effect at least nine of the systems have other indicators of increased chromospheric and magnetic activity.

Unified Astronomy Thesaurus concepts: Contact binary stars (297); Orbital elements (1177); Transient detection (1957)

1. Introduction

As the number of identified contact binary systems grows with new discoveries from an ever growing number of sky surveys, the interest in their investigation has also increased. The confirmation of Nova 2008 Sco (V1390 Sco) as a red nova resulting from the merger of contact binary components (Tylenda et al. 2011) has also intensified interest in the investigation of orbital stability of contact binary systems (Gazeas et al. 2021; Wadhwa et al. 2021; Christopoulou et al. 2022; Liu et al. 2023). Theoretical models of contact binary evolution predict a likely merger event leading to a rapidly rotating cool giant star as the final outcome (Robertson & Eggleton 1977; Soker & Tylenda 2003; Stepień 2011; Eggleton 2012). Although the predicted rate of Galactic merger events is high at once every 2–3 yr, brighter events suitable for study are likely to be much rarer at once every 10 or more years (Kochanek et al. 2014).

Investigators such Rasio & Shapiro (1995), Li et al. (2007) and Arbutina (2007, 2009) have clearly shown that merger events are likely to occur when the mass ratio of the components is low. More recently Wadhwa et al. (2021) linked the instability parameters to the mass of the primary (M_1) and concluded that there is not one global minimum mass ratio at which merger will take place, rather the instability mass ratio can range from below 0.05 to above 0.2 for systems where $0.6M_\odot < M_1 < 1.4M_\odot$. Although a number of studies, each with a large (10 or greater) number of contact binaries with extremely low mass ratios, have recently been reported they did not identify any system that meet the instability criteria (Gazeas et al. 2021; Christopoulou et al. 2022; Li et al. 2022; Liu et al. 2023). Wadhwa et al. (2022) recently linked the amplitude of totally eclipsing contact binaries with the mass ratio which when used in conjunction with estimates of the mass of the primary can result in the rapid identification of potentially unstable systems. They identified over 40 new potential merger candidates based on the analysis of survey photometric data. In this study we perform follow up ground based observations on nine systems identified by Wadhwa et al. (2022) and three other systems identified from the All Sky Automated Survey—Super Nova (ASAS-SN) (Shappee et al. 2014; Jayasinghe et al. 2020) using the criteria described in Wadhwa et al. (2022). Basic identification data for each system is presented in Table 1. Almost all ground based surveys have been carried out using either small aperture telescopes or telephoto lenses. The angular resolution is therefore quite poor ranging from 9″ to over 60″ (Shappee et al. 2014; Drake et al. 2017; Jayasinghe et al. 2020; Pojmanski 2002; Thiemann et al. 2021). The risk of potential blending of the survey light curves was highlighted by Wadhwa et al. (2023) where a system thought to be of extreme low mass ratio and a potential merger candidate is in fact a high mass ratio system with no indications of orbital instability. Each system reported here was checked against Gaia EDR 3 (Anders et al. 2022; Gaia Collaboration et al. 2023) to ensure there was no other star system brighter than 17th magnitude within 10″ of the target. We perform light curve analysis and compare our results with reported data from survey analysis, in addition, we show that all systems described demonstrate features of orbital instability, have secondaries that are denser

Table 1
Name, Abbreviations (Used in all other Tables and Text) along with Comparison and Check Stars for 12 Contact Binary Systems

Name	Abbreviation	Comparison Star	Check Star
ASAS J045814+0643.1	A0458	TYC 97-681-1	TYC 97-273-1
ASAS J051459-7356.3	A0514	TYC 9174-356-1	2MASS 05140657-7351334
ASAS J100101-7958.6	A1001	TYC 9404-105-1	2MASS 09593687-7954508
V396 Lup	V396 Lup	TYC 7851-983-1	2MASS16031759-3751375
ASAS J170715-5118.7	A1707	TYC 8340-637-1	2MASS 17072965-5118000
ASAS J184644-2736.4	A1846	TYC 6867-2234-1	TYC 6867-2250-1
ASAS J202231-4452.5	A2022	TYC 7961-1064-1	TYC 7961-842-1
ASAS J204452+0622.6	A2044	2MASS 20445329+0619549	2MASS 20444317+0619507
ASAS J213219-5351.6	A2132	UCAC2 8680692	UCAC4 181-218564
SSS-J221327.1-445401	S2213	UCAC2 12815832	2MASS 22140108-4453567
ASAS J225826-2603.6	A2258	TYC 6974-1080-1	TYC 6974-880-1
ASAS J234823-4054.7	A2348	TYC 8018-55-1	2MASS 23480833-4046082

Table 2
Observation Dates, Number of Observations, Exposure Times, Light Curve Parameters and Spectral Classification of the Twelve Reported Contact Binary Systems

Name	Obs Date	Obs (V, R)	Exp Times (V, R)	Max (V)	Ampl (V)	$B-V$	M_{V1}	$M_1/M_\odot$
A0458	11/21–01/23	285, 350	45 s, 45 s	11.76	0.26	0.46	3.88 ± 0.01	1.17 ± 0.02
A0514	01/22–10/22	320, 300	45 s, 45 s	11.71	0.37	0.71	4.90 ± 0.02	0.98 ± 0.01
A1001	04/20–04/20	373, 375	40 s, 40 s	11.47	0.33	0.91	5.78 ± 0.01	0.83 ± 0.01
V396 Lup	06/21–07/21	670, 240	30 s, 25 s	10.88	0.36	0.83	5.20 ± 0.02	0.95 ± 0.01
A1707	07/21–08/21	510, 500	40 s, 35 s	11.19	0.44	0.55	3.67 ± 0.02	1.22 ± 0.01
A1846	08/21–08/21	300, 410	40 s, 40 s	11.78	0.39	0.78	5.43 ± 0.02	0.90 ± 0.01
A2022	08/21–08/21	550, 300	45 s, 45 s	12.09	0.31	0.53	4.38 ± 0.01	1.11 ± 0.01
A2044	08/22–10/22	440, 280	50 s, 45 s	12.67	0.30	0.62	4.18 ± 0.02	1.13 ± 0.01
A2132	10/21–09/22	255, 250	55 s, 55 s	12.89	0.28	0.55	4.48 ± 0.02	1.04 ± 0.01
S2213	09/21–09/21	250, 300	45 s, 45 s	12.49	0.27	0.55	4.05 ± 0.02	1.15 ± 0.02
A2258	09/21–10/21	255, 330	35 s, 35 s	11.49	0.26	0.60	4.21 ± 0.02	1.12 ± 0.01
A2348	11/21–08/22	350, 350	50 s, 50 s	12.83	0.30	0.54	4.16 ± 0.03	1.11 ± 0.02

Note. A1001, V396 Lup, A1707 and A1846 were observed with the WSU telescope others through the LCO telescope network. * = Spectral classification from published literature.

and most show evidence of chromospheric activity in the absence of star spots.

2. Photometric Observations, Absolute Magnitudes and Mass of the Primary Component

2.1. Photometric Observations

We acquired dual band (V and R) images of 12 contact binary systems from 2020 April to 2023 January using either the 0.6 m Western Sydney University (WSU) telescope equipped with a cooled SBIG 8300 CCD camera and standard Johnson *BVR* filters or the 0.4 m telescopes of the Las Cumbres Observatory (LCO) network equipped with SBIG STL-6303 CCD camera and Bessel V, B and Sloan r' filters. In addition to V and R band images, B band images were obtained only during eclipses to document $B-V$ magnitude for each system. The LCO network automatically calibrates all images while the images obtained at the WSU were calibrated with multiple flat, dark and bias frames. Differential photometry was performed for each system using the AstroImageJ (Collins et al. 2017) software package. All observations with software reported error of greater than 0.01 mag were excluded. Observation dates, number of observations, exposure times, maximum V band brightness, V Band amplitude and $B-V$ magnitude are summarized in Table 2.

Based on the times of minima observed and available V band photometric data from the ASAS-SN and All Sky Automated Survey (ASAS) (Pojmanski 2002) we updated the orbital elements as summerized in Table 3.

2.2. Absolute Magnitude of the Primary Component

As all systems described have a very low mass ratio (see below) and all demonstrate total eclipses we are presented with a prospect of being able to estimate the absolute magnitude of the primary component using direct observations. The apparent magnitude of the secondary eclipse represents the apparent

Table 3
Updated Orbital Elements

Name	Epoch (HJD)	Period (days)
A0458	2459543.900671 ± 0.000728	0.333482 ± 0.000012
A0514	2459594.108439 ± 0.000520	0.345729 ± 0.000085
A1001	2458961.971160 ± 0.000920	0.279133 ± 0.000085
V396 Lup	2459372.012959 ± 0.000420	0.363248 ± 0.000060
A1707	2459430.984062 ± 0.000511	0.525901 ± 0.000040
A1846	2459439.005458 ± 0.000225	0.302853 ± 0.000030
A2022	2459429.668598 ± 0.000986	0.345011 ± 0.000006
A2044	2459818.566466 ± 0.000564	0.370536 ± 0.000029
A2132	2459509.962001 ± 0.000488	0.316348 ± 0.000058
S2213	2459459.704234 ± 0.000621	0.369894 ± 0.000005
A2258	2459436.659418 ± 0.000267	0.327648 ± 0.000060
A2348	2459545.581557 ± 0.000223	0.347195 ± 0.000052

magnitude of the primary. If the distance is known, the absolute magnitude of the primary (M_{V1}) can be estimated as follows:

$$M = m - 5\log_{10} d + 5. \quad (1)$$

Where M is the absolute magnitude, m is the apparent magnitude and d is the distance in parsecs.

The GAIA mission (Anders et al. 2022) provides highly accurate estimates of the distance particularly of nearby stars and as such makes distance based estimate of the absolute magnitude a reality. Interstellar extinction however must be taken into consideration when determining the apparent magnitude. As most dust maps report line of sight extinction to infinity and all our systems have distance estimations well below 1 kpc we corrected the extinction for distance as follows: Using Schlafly & Finkbeiner (2011) dust maps we determined the line of sight reddening at infinity $E(B-V)_\infty$. We used the Gaia distance to scale this value $E(B-V)_d$ using the equation (Bilir et al. 2008):

$$E(B-V)_d = E(B-V)_\infty \left[1 - \exp\left(-\frac{|d \cdot \sin(b)|}{h}\right)\right]. \quad (2)$$

In the equation b is the galactic latitude of the system, d is the Gaia distance (in parsecs) and h is the galactic scale height, taken as $h = 125$ pc as per Bilir et al. (2008). The total extinction (A_V) was then estimated as $A_V = E(B-V)_d \times 3.1$.

The estimated absolute magnitude for each system is summarized in Table 2. The largest contributor to the estimated error in the absolute magnitude was the reported error in the distance estimate.

2.3. Mass of the Primary Component

One of the main aims of this report is to assess potential orbital instability of the reported contact binary systems. Recently, Wadhwa et al. (2021) developed new relationships linking the mass of the primary (M_1), the degree of contact and the instability mass ratio (q_{inst}). One can estimate the range of mass ratios over which a system may become unstable if the mass of the primary is known. Direct estimation of the mass of the primary is not possible, one is therefore reliant on secondary observations and calibrations. Primary components of contact binary systems follow a main sequence profile (Yildiz & Doğan 2013). For this study we use two methods to estimate the mass of the primary. The Two Micron All Sky Survey (2MASS) (Skrutskie et al. 2006) acquired simultaneous photometry in multiple infrared bands. As our first estimate of the mass of the primary we used the 2MASS $J-H$ magnitudes and the 2022 April update tables of Pecaut & Mamajek (2013) for low mass ($0.6M_\odot < M_1 < 1.4M_\odot$) main sequence stars to interpolate the mass of the primary. Our distance based estimate is linked to the absolute magnitude of the primary determined above. Again we use the 2022 April update tables of Pecaut & Mamajek (2013) for low mass ($0.6M_\odot < M_1 < 1.4M_\odot$) main sequence stars to interpolate the mass of the primary. We use the mean of the color and distance based estimates as our adopted value for the mass of the primary. The recorded errors were propagated when calculating the instability mass ratio range (see below). Summary results for the mass of the primary are recorded in Table 2.

3. Light Curve Analysis and the Mass Ratio

Having established an estimate for the mass of the primary the next (and only) other parameter required to determine potential orbital stability is the mass ratio of the system. In the absence of radial velocity measurements light curve analysis of contact binary systems can be successfully carried out if total eclipses are present (Terrell & Wilson 2005). One of the input parameters for such analysis is the temperature of the primary component (T_1). There is no standard method for assigning the value for the temperature of the primary. Color based estimations have been the mainstream, however these have proven troublesome, for example the ViziR database reports a range of over 3000 K for one of our targets (V396 Lup). Given the lack of a standard approach many investigators (see e.g., Zhou et al. 2018; Chang et al. 2022; Guo et al. 2022) are now moving to low resolution spectra (where available) to aid in determining the primary's temperature. To this end for this study we acquired spectra using the LCO network of 2 m telescopes equipped with FLOYDS spectrograph, a cross-dispersed, spectrograph with variable resolution of $R = 400$ to $R = 700$ for 10 of the systems. The reduction pipeline for the FLOYDS spectral data is fully automated and described in detail on the LCO website (https://lco.global/documentation/data/floyds-pipeline/—accessed 2023 January 14). For A0514 we used the published spectral data (Cannon & Pickering 1993). We were unable to obtain a spectrum for A2044 due to technical reasons during the allotted time. All FLOYDS spectra were visually compared to standard library spectra of main sequence stars (Jacoby et al. 1984; Pickles 1998) to determine

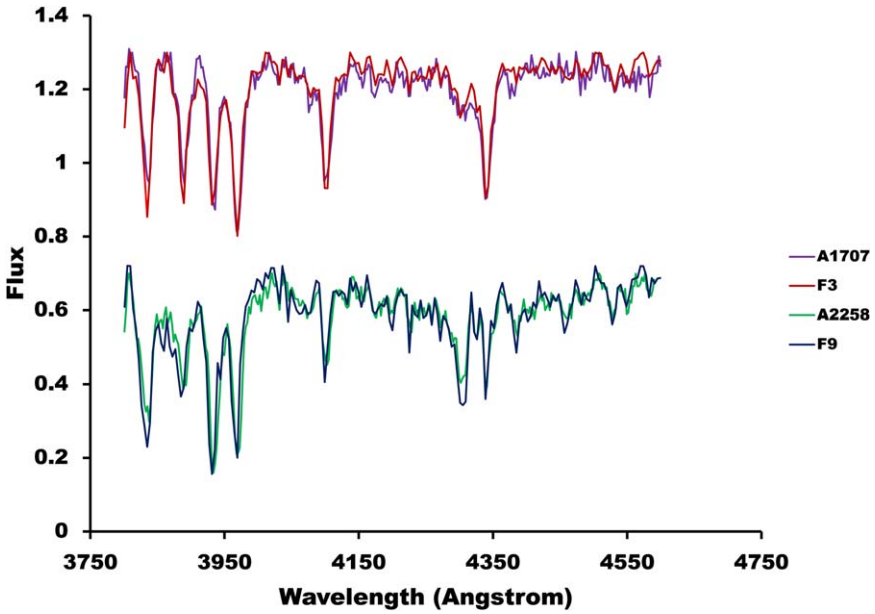

Figure 1. The low resolution FLOYDS spectra were visually matched to standard main sequence star spectra to determine the spectral class for 10 of the systems.

Table 4
Effective Temperatures Based on $B-V$, $J-H$, Spectral Class and GAIA

Name	$B-V$(K)	$J-H$(K)	Sp(K)	GAIA(K)	Mean ± SD	Sp Class
A0458	6650	6060	7020	7110	6710 ± 410	F1
A0514	5810	5600	5930	5310	5660 ± 240	G0[a]
A1001	5140	4870	5380	4990	5100 ± 190	G9
V396 Lup	5520	5550	6050	5930	5760 ± 230	F9
A1707	6610	6190	6750	6550	6530 ± 210	F3
A1846	5530	5370	5550	5080	5380 ± 190	G7
A2022	6280	6060	5930	6240	6130 ± 140	G0
A2044	6070	6060	…	5900	6010 ± 80	…
A2132	6190	5710	6180	6020	6030 ± 190	F8
S2213	6190	6060	6280	5970	6130 ± 120	F7
A2258	6000	5990	6050	5910	5990 ± 50	F9
A2348	6180	5930	6550	6110	6190 ± 230	F5

Notes. Mean Value ±(SD) was the Adopted Value for Light Curve Analysis. In the last column we record the spectral class for each system.
[a] In the case of A0514 we use the published data (Cannon & Pickering 1993).

the spectral class for each system. Representative FLOYDS spectra and matching library spectra are shown in Figure 1.

For this study we use the mean (±SD) of four estimates for the temperature of the primary. We estimate effective temperature of the primary based on our extinction corrected value of $B-V$, the observed spectral class, the 2MASS $J-H$ color and the reported value from the GAIA third data release all adjusted to the nearest 10. For consistency we use the 2022 April update tables of Pecaut & Mamajek (2013) for color and spectral calibrations. Summary of the spectral class, temperatures and the adopted mean value of the four calibrations is presented in Table 4. In the case of A2044 where no spectral observations were available we adopt the mean of the two color calibrations and the GAIA estimate.

The 2013 version of the Wilson–Devinney (WD) code with Kurucz atmospheres (Wilson 1990; Kallrath et al. 1998; Nelson 2021) was used to obtain the photometric solution for each system. As all systems show total eclipses accurate photometric solutions are possible and as there was no significant asymmetry at maximum brightness (i.e., no significant O'Connell Effect) only unspotted solutions were obtained. As the effective temperature of the primary is less than 7200 K in all cases, the gravity coefficients were set as $g_1 = g_2 = 0.32$, and bolometric albedoes as $A_1 = A_2 = 0.5$. Logarithmic

(Nelson & Robb 2015) limb darkening coefficients were interpolated from the 2019 update of van Hamme (1993).

Simultaneous solutions were obtained for both the V and R band in all cases. Mass ratio (q) search grid method was used to find the best solution for a range of fixed mass ratios from 0.05 to 20. The initial search was performed with mass ratio increments of 0.1 up to $q = 1$ and then 0.2 up to $q = 10$ and 0.5 increments up to $q = 20$. The search was then refined near the best solution in increments of 0.05 and finally in increments of 0.01. During the search procedure the orbital inclination (i), the surface potential, temperature of the secondary component (T_2) and the dimensionless luminosity of the primary (L_1) were the adjustable parameters and all of which were adjusted between each iteration. The iterations were carried out until the suggested adjustment for all adjustable parameters was less than the reported standard deviation. During the last iteration the mass ratio was also made a adjustable parameter.

To determine the effects of the variable temperature of the primary each system was further modeled with mass ratio increments of 0.01 around the mean temperature solution with the temperature of the primary adjusted both to the upper and lower limits reported in Table 4. As has been well established the light curve shape of contact binaries is almost completely due to the system geometry with the degree of contact, mass ratio and inclination being the major contributors (Rucinski 1993, 2001). The shape of contact binary light curves places a tight constrain on the component temperature ratio (T_2/T_1) but not on individual component temperatures (Rucinski 1993; Sun et al. 2020). With change in T_1 we expected change in T_2 but no significant change in the geometric parameters. This proved to be the case with the light curve solution converging to the same mass ratio regardless of the input value of T_1 except in the case of A1846 where the mean T_1 solution converged at $q = 0.151$ and the higher T_1 solution converged at $q = 0.150$. Similarly the inclination variation between high, mean and low values for T_1 were within $0^{\circ}.5$ and within the reported standard deviations reported by the WD software. The dimensionless potential and the geometric mean of the fractional radii again varied minimally. Although the errors in geometric parameters were small with change in temperature of the primary they were propagated to the mean solution reported. Apart from the mass ratio and fractional radii (reported to two decimal places) no other parameter resulting from modeling of the light curve is further used in this study. We report light curve solution parameters pertinent to this study in Table 5 with errors propagated relative to the input errors in T_1. Fitted and observed light curves are illustrated in Figure 2.

4. Orbital Stability

Orbital stability and potential merger of contact binary systems has received considerable attention recently (Wadhwa et al. 2021; Christopoulou et al. 2022; Liu et al. 2023). Wadhwa et al. (2021) developed new relationships linking the mass of the primary, the degree of contact and the instability mass ratio ($q_{\rm inst}$). Following their methodology, and adopting the values of the gyration radii of the components as described, we calculated $q_{\rm inst}$ for each system for fill-out factor values of 0 and 1 (Table 5). This provides a range of mass ratios where orbital instability is likely. As noted by Christopoulou et al. (2022) a small uncertainty in the estimation of the mass of the primary propagates to a significant uncertainty in the estimation of orbital instability parameters. This is confirmed by this study where the mean mass of the primary components of the systems presented in this study is $1.06 M_{\odot}$. At this mass the instability mass ratio range for fill-out factor 0 to 1 extends from 0.094 to 0.109. A 10% change in the mass of the primary (either above or below) results in a greater than 17% change in the instability mass ratio range. Thus for the purpose of this study we consider any system where the mass ratio is within 17% of the maximum instability mass ratio to be potentially unstable. Based on this criteria ten of the twelve systems lie within the instability mass ratio range taking into account reported errors. One (A1846) is within 7% and one (A2348) 17% of the maximum instability mass ratio. We note that the distance estimation of A2348 has a reported error near 10% so we consider it reasonable to include the system as potentially unstable. The instability mass ratio ranges are summarized in Table 5.

Manual analysis of the survey photometric data for 9 of the systems presented here was reported by Wadhwa et al. (2022). The survey data mass ratio estimate was within 10% of the mass ratio based on dedicated observations except in the case of A2044 and A2132 where the survey data estimates of the mass ratio were 20% and 12%, respectively, below the values reported here.The findings confirm that generally survey photometric data provides a good starting point in the selection of potential low mass ratio systems and merger candidates. Wadhwa et al. (2022) found that all 9 of the common systems could be regarded as potential merger candidates as their estimation of the mass of the primary was based on $J - H$ calibration. Looking at the two candidates in our report A1846 and A2348 which are just outside the instability range, have $J - H$ calibrated mass of the primary, 0.89 and 1.07, respectively, both lower than the combined with distance estimation used in this study. If the single color estimation was used than the 2 would fall within the instability range.

5. Density and Chromospheric Activity

5.1. Component Density

It is well known that the secondary components are larger than their main sequence counterparts. In addition to change in the radius some researchers (Yildiz & Doğan 2013) postulate that distortions of the secondary may result from it actually

Table 5
Light Curve Solution Summary of the Main Pertinent Parameters

Name	T_1(K)	T_2(K)	Incl (°)	Mass Ratio (q)	Fr Radii ($r_{1,2}$)	$q_{\rm inst}$ Range
A0458	6710 ± 410	6190 ± 380	88.4 ± 0.8	0.089 ± 0.001	0.60 ± 0.01, 0.21 ± 0.01	0.079 ± 0.003–0.09 ± 0.003
A0514	5660 ± 240	5820 ± 240	73.5 ± 0.6	0.12 ± 0.001	0.59 ± 0.01, 0.26 ± 0.01	0.105 ± 0.002–0.123 ± 0.002
A1001	5100 ± 190	4960 ± 180	72.4 ± 0.7	0.138 ± 0.003	0.56 ± 0.01, 0.24 ± 0.01	0.129 ± 0.002–0.155 ± 0.002
V396 Lup	5760 ± 230	5670 ± 230	78.0 ± 0.4	0.133 ± 0.002	0.58 ± 0.01, 0.26 ± 0.01	0.110 ± 0.002–0.130 ± 0.002
A1707	6530 ± 210	6080 ± 190	80.8 ± 0.6	0.072 ± 0.002	0.62 ± 0.01, 0.21 ± 0.01	0.072 ± 0.002–0.082 ± 0.002
A1846	5380 ± 190	5720 ± 210	87.0 ± 0.7	0.150 ± 0.002	0.56 ± 0.01, 0.25 ± 0.01	0.117 ± 0.001–0.140 ± 0.002
A2022	6130 ± 140	6260 ± 150	80.1 ± 0.7	0.100 ± 0.003	0.60 ± 0.01, 0.24 ± 0.01	0.087 ± 0.002–0.100 ± 0.002
A2044	6010 ± 80	5940 ± 80	87.2 ± 0.6	0.088 ± 0.001	0.61 ± 0.01, 0.22 ± 0.01	0.084 ± 0.003–0.097 ± 0.004
A2132	6030 ± 190	6040 ± 190	73.4 ± 0.5	0.113 ± 0.002	0.58 ± 0.01, 0.23 ± 0.01	0.096 ± 0.001–0.112 ± 0.002
S2213	6130 ± 120	5960 ± 120	$90.00^{+0.00}_{-1.5}$	0.088 ± 0.003	0.61 ± 0.01, 0.22 ± 0.01	0.081 ± 0.003–0.093 ± 0.003
A2258	5990 ± 50	5970 ± 50	$90.00^{+0.00}_{-0.6}$	0.087 ± 0.002	0.57 ± 0.01, 0.22 ± 0.01	0.081 ± 0.003–0.098 ± 0.002
A2348	6190 ± 230	6070 ± 220	73.9 ± 0.5	0.117 ± 0.002	0.59 ± 0.01, 0.24 ± 0.01	0.087 ± 0.003–0.100 ± 0.003

Note. ($r_{1,2}$) = geometric fractional radii and ($q_{\rm inst}$) = the instability mass ratio range.

being initially a larger primary that has lost mass to the current primary and due to retention of higher mass core constituents is likely to be denser than the primary. Kähler (2004) argues that the densities of the components will always be different and that the difference between density of the primary (ρ_1) and that of the secondary (ρ_2) will always be negative.

As noted by Mochnacki (1981) the density of the components in (g cm^{-3}) can be expressed as a function of the period, relative radii and mass ratio. The density difference ($\Delta\rho$) between the components can be expressed as:

$$\Delta\rho = \frac{0.0189}{r_1^3(1+q)P^2} - \frac{0.0189q}{r_2^3(1+q)P^2}. \quad (3)$$

All our system confirm the finding that the secondary is much denser and that $\Delta\rho$ is negative. The findings (to two decimal places) are summerized in Table 6.

5.2. Chromospheric Activity

Contact binary systems typically have synchronised rotation with short periods of less than 1 day. Such rapid rotation rates are thought to increase magnetic activity related to contact binary systems (Gharami et al. 2019). Increased magnetic activity may manifest itself as magnetic stellar wind and magnetic breaking leading to loss of angular momentum from the system (Li et al. 2004). Although it is difficult to directly measure angular momentum loss there are potential secondary indicators of increased magnetic activity, such as strong ultraviolet emissions and/or increased chromospheric activity (Rucinski & Vilhu 1983; Vilhu 1983; Li et al. 2004). There are some chromospheric and magnetic signals associated with contact binaries with the most readily observed light curve feature being the asymmetry in the maxima (O'Connell effect). Apart from the O'Connell effect and incorporation of starspots, the analysis of light curves provides little indication of chromospheric activity. None of the systems described in this report show significant variation of maxima, however, that does not exclude the presence of significant magnetic and chromospheric activity. High energy spectral emissions provide a much clearer indicators of enhanced chromospheric/magnetic activity. In low mass dwarfs the chromospheric emissions are by photospheric light in the visual band. Higher energy emissions particularly in the far-ultraviolet region provide a less obscured alternative (Smith & Redenbaugh 2010). The Galaxy Evolution Explorer (GALEX) satellite imaged the sky in the far-ultraviolet band (FUV) centered on 1539 Å and this can be employed to explore chromospheric activity of contact binaries (Smith & Redenbaugh 2010).

The $R'_{\rm HK}$ index (Noyes et al. 1984) is an excepted measure of chromospheric emission strength with $\log R'_{\rm HK} \geqslant -4.75$ characteristic of a more active star (Henry et al. 1996). Smith & Redenbaugh (2010) matched GALEX FUV magnitudes ($m_{\rm FUV}$) to the $\log R'_{\rm HK}$ for dwarf stars to derive the $\Delta(m_{\rm FUV-B})$ color excess:

$$\Delta(m_{\rm FUV-B}) = (m_{\rm FUV} - B) - (m_{\rm FUV} - B)_{\rm base} \quad (4)$$

where

$$(m_{\rm FUV} - B)_{\rm base} = 6.73(B - V) + 7.43. \quad (5)$$

They deduced that for active stars the color excess was always below -0.5 and often less than -1.0. Less active stars usually had color excess well above -0.5.

Six of our twelve systems were observed by the GALEX mission with recorded FUV magnitudes. We calculated the color excess for all six using the above relationships and show that all have an ultraviolet color excess well below -0.5 indicative of significant chromospheric/magnetic activity in the absence of light curve features. Magnetically active features, sometimes referred to as plages (Hall 2008), are responsible for the chromospheric emissions while starspots are regions of intense magnetic activity leading to suppression of convection in the photosphere (Solanki 2003). Although starspots are

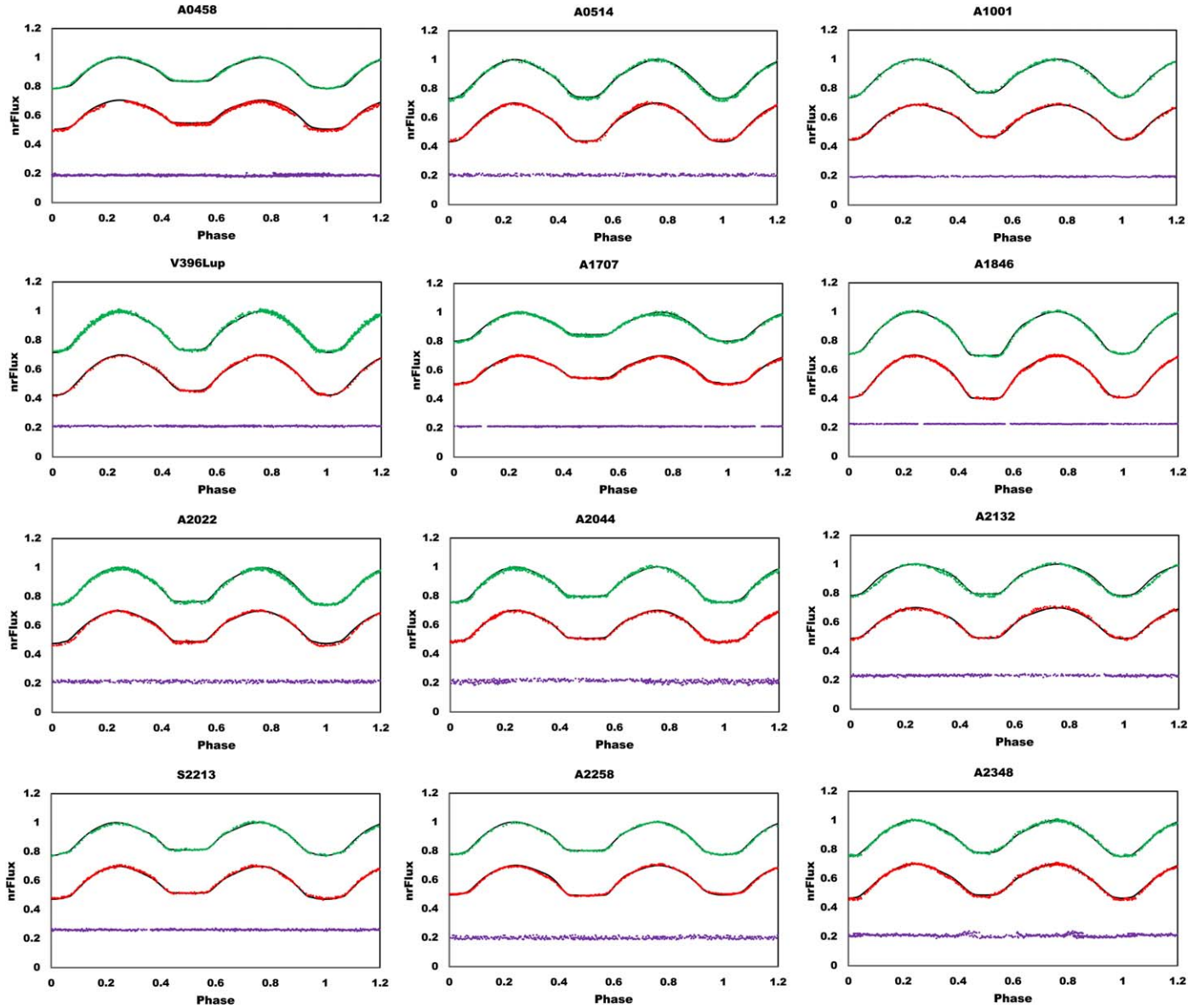

Figure 2. Observed and modeled light curves for the 12 systems. The green and red light curves represent the V and $R(r')$ bands while the purple curve represents the check star. The black line represents the WD modeled curve. The vertical axis labeled nrFlux represents the normalized flux which has been arbitrarily shifted vertically for clarity.

accompanied by plague regions, the reverse is not always true such that chromospheric activity is possible without photospheric starspots (Mandal et al. 2017). The UV color excesses are summarized in Table 6.

Coronal and chromospheric activity combined with fast synchronous rotation of the common envelopes may also result in X-Ray emissions from contact binaries (Gondoin 2004; Kandulapati et al. 2015). Seven of our systems (A0458, A0514, V396 Lup, A1846, A2044, S2213, A2348) were reported as potential X-Ray sources (Liu et al. 2022) including three (A0514, V396 Lup and A2044) without FUV observations bringing to a total of nine systems with signs suggestive of increased chromospheric activity without characteristic photospheric changes.

6. Discussion and Conclusion

Photometric observations and light curve solution of twelve low mass contact binary systems is presented. All were found to be of extreme low mass ratio ranging from 0.072 to 0.15. Compared to theoretical parameters all have a mass ratios indicative of likely orbital instability and are likely merger (red

Table 6
Density and Ultraviolet Color Excess

Name	ρ_1(g cm^{-3})	ρ_2(g cm^{-3})	$\Delta\rho$	$\Delta(m_{\rm FUV} - B)$
A0458	0.72 ± 0.01	1.49 ± 0.01	−0.77	−3.34
A0514	0.69 ± 0.01	0.96 ± 0.01	−0.27	⋯
A1001	1.21 ± 0.02	2.13 ± 0.02	−0.92	⋯
V396 Lup	0.65 ± 0.03	0.96 ± 0.02	−0.31	⋯
A1707	0.27 ± 0.01	0.50 ± 0.02	−0.23	⋯
A1846	1.02 ± 0.01	1.72 ± 0.02	−0.70	⋯
A2022	0.67 ± 0.02	1.04 ± 0.02	−0.37	−2.30
A2044	0.56 ± 0.01	1.05 ± 0.01	−0.49	⋯
A2132	0.87 ± 0.02	1.58 ± 0.02	−0.71	−2.80
S2213	0.56 ± 0.01	1.05 ± 0.02	−0.49	−2.32
A2258	0.87 ± 0.01	1.32 ± 0.02	−0.45	−2.56
A2348	0.68 ± 0.01	1.19 ± 0.02	−0.51	−3.23

nova) candidates. Regular high cadence future observations are encouraged to accurately determine period variations and brightness changes which maybe an indicator of impending merger (Tylenda et al. 2011). A thorough study of orbital behavior of contact binaries have been performed recently by Zhang & Qian (2020), Poro et al. (2022), Loukaidou et al. (2022). The first and the last paper discuss in particular the systems close to the orbital period cut-of. Ultra-short period systems seem to have generally stable orbits and do not show evidence of significant period decrease. From the viewpoint of Darwin instability, this is understandable, since these are not such a low-mass ratio systems and it may take a long evolutionary time for ultra-short contact binaries to reach an extremely low mass ratio and become dynamically unstable (Loukaidou et al. 2022).

Review of some astrophysical characteristics confirm similarity with other contact binary systems with the secondary considerably brighter and larger than main sequence stars of similar mass. In addition, the secondary in all cases is significantly denser than the current primary. Chromospheric activity in contact binary is usually detected as a variation in the two maxima from the light curve due to starspots. As we have shown in this study non-photospheric markers probably can detect such activity without typical light curve features. Another high energy feature of excess chromospheric/magnetic activity is X-Ray emissions (Gondoin 2004). Only a small fraction of contact binary star systems are X-ray sources (Liu et al. 2022) such that presence of X-Ray emissions can be taken as a marker of increased magnetic activity and potential indicator for an increased loss of angular momentum and orbital instability. Seven of twelve systems reported have been cataloged as having X-Ray emissions (Liu et al. 2022). Also, as noted above the FUV magnitude can be used as a marker for chromospheric activity. Another interesting point of note is how much brighter relative to main sequence stars are the contact binaries in the FUV band. Findeisen & Hillenbrand (2010) have estimated the absolute FUV magnitudes ($M_{\rm FMS}$) for single main sequence stars from B8 to M2 spectral types. For the six systems from our sample with FUV magnitude we find that all systems are between 0.5 and over 3.0 mag brighter in the FUV band relative to their main sequence counterparts.

Progress in the detection and monitoring of potential contact binary merger candidates is rapidly progressing. There now exists a theoretical framework to determine the potential for merger from the estimate of the mass of the primary and the mass ratio of the system (Wadhwa et al. 2021). Models and techniques have been developed to rapidly select potential merger candidates from survey photometry (Wadhwa et al. 2022). However, follow up dedicated observations are required due to the low resolution of most survey data (Wadhwa et al. 2023).

Acknowledgments

Based on data acquired on the Western Sydney University, Penrith Observatory Telescope. We acknowledge the traditional custodians of the land on which the Observatory stands, the Dharug people, and pay our respects to elders past and present.

This research has made use of the SIMBAD database, operated at CDS, Strasbourg, France.

This research has made use of the VizieR catalog access tool, CDS, Strasbourg, France (DOI:10.26093/cds/vizier).

B. Arbutina, G. Djurašević and J. Petrović acknowledge the funding provided by the Ministry of Science, Technological Development and Innovation of the Republic of Serbia through the contracts 451-03-47/2023-01/200104 (B.A.) and 451-03-47/2023-01/200002 (GDj, JP).

ORCID iDs

Surjit S. Wadhwa https://orcid.org/0000-0002-7011-7541
Bojan Arbutina https://orcid.org/0000-0002-8036-4132
Nick F. H. Tothill https://orcid.org/0000-0002-9931-5162
Miroslav D. Filipović https://orcid.org/0000-0002-4990-9288
Ain Y. De Horta https://orcid.org/0000-0001-9677-1499
Jelena Petrović https://orcid.org/0000-0001-8535-7807
Gojko Djurašević https://orcid.org/0000-0001-9392-6678

References

Anders, F., Khalatyan, A., Queiroz, A. B. A., et al. 2022, A&A, 658, A91
Arbutina, B. 2007, MNRAS, 377, 1635
Arbutina, B. 2009, MNRAS, 394, 501
Bilir, S., Ak, S., Karaali, S., et al. 2008, MNRAS, 384, 1178
Cannon, A. J., & Pickering, E. C. 1993, yCat, III/135A
Chang, L.-F., Zhu, L.-Y., Sarotsakulchai, T., & Soonthornthum, B. 2022, PASJ, 74, 1421
Christopoulou, P.-E., Lalounta, E., Papageorgiou, A., et al. 2022, MNRAS, 512, 1244
Collins, K. A., Kielkopf, J. F., Stassun, K. G., & Hessman, F. V. 2017, AJ, 153, 77
Drake, A. J., Djorgovski, S. G., Catelan, M., et al. 2017, MNRAS, 469, 3688

Eggleton, P. P. 2012, JASS, 29, 145
Findeisen, K., & Hillenbrand, L. 2010, AJ, 139, 1338
Gaia Collaboration, Vallenari, A., & Brown, A. G. A. 2023, A&A, 674, A1
Gazeas, K. D., Loukaidou, G. A., Niarchos, P. G., et al. 2021, MNRAS, 502, 2879
Gharami, P., Ghosh, K., & Rahaman, F. 2019, BlgAJ, 31, 97
Gondoin, P. 2004, A&A, 415, 1113
Guo, D.-F., Li, K., Liu, F., et al. 2022, MNRAS, 517, 1928
Hall, J. C. 2008, LRSP, 5, 2
Henry, T. J., Soderblom, D. R., Donahue, R. A., & Baliunas, S. L. 1996, AJ, 111, 439
Jacoby, G. H., Hunter, D. A., & Christian, C. A. 1984, ApJS, 56, 257
Jayasinghe, T., Stanek, K. Z., Kochanek, C. S., et al. 2020, MNRAS, 491, 13
Kähler, H. 2004, A&A, 414, 317
Kallrath, J., Milone, E. F., Terrell, D., & Young, A. T. 1998, ApJ, 508, 308
Kandulapati, S., Devarapalli, S. P., & Pasagada, V. R. 2015, MNRAS, 446, 510
Kochanek, C. S., Adams, S. M., & Belczynski, K. 2014, MNRAS, 443, 1319
Li, K., Gao, X., Liu, X.-Y., et al. 2022, AJ, 164, 202
Li, L., Han, Z., & Zhang, F. 2004, MNRAS, 355, 1383
Li, L., Zhang, F., Han, Z., & Jiang, D. 2007, ApJ, 662, 596
Liu, J., Wu, J., Esamdin, A., et al. 2022, A&A, 663, A115
Liu, X.-Y., Li, K., Michel, R., et al. 2023, MNRAS, 519, 5760
Loukaidou, G. A., Gazeas, K. D., Palafouta, S., et al. 2022, MNRAS, 514, 5528
Mandal, S., Chatterjee, S., & Banerjee, D. 2017, ApJ, 835, 158
Mochnacki, S. W. 1981, ApJ, 245, 650
Nelson, R. H. 2021, NewA, 86, 101565
Nelson, R. H., & Robb, R. M. 2015, IBVS, 6134, 1
Noyes, R. W., Hartmann, L. W., Baliunas, S. L., Duncan, D. K., & Vaughan, A. H. 1984, ApJ, 279, 763
Pecaut, M. J., & Mamajek, E. E. 2013, ApJS, 208, 9
Pickles, A. J. 1998, PASP, 110, 863
Pojmanski, G. 2002, AcA, 52, 397
Poro, A., Sarabi, S., Zamanpour, S., et al. 2022, MNRAS, 510, 5315
Rasio, F. A., & Shapiro, S. L. 1995, ApJ, 438, 887
Robertson, J. A., & Eggleton, P. P. 1977, MNRAS, 179, 359
Rucinski, S. M. 1993, PASP, 105, 1433
Rucinski, S. M. 2001, AJ, 122, 1007
Rucinski, S. M., & Vilhu, O. 1983, MNRAS, 202, 1221
Schlafly, E. F., & Finkbeiner, D. P. 2011, ApJ, 737, 103
Shappee, B. J., Prieto, J. L., Grupe, D., et al. 2014, ApJ, 788, 48
Skrutskie, M. F., Cutri, R. M., Stiening, R., et al. 2006, AJ, 131, 1163
Smith, G. H., & Redenbaugh, A. K. 2010, PASP, 122, 1303
Soker, N., & Tylenda, R. 2003, ApJL, 582, L105
Solanki, S. K. 2003, A&ARv, 11, 153
Stępień, K. 2011, A&A, 531, A18
Sun, W., Chen, X., Deng, L., & de Grijs, R. 2020, ApJS, 247, 50
Terrell, D., & Wilson, R. E. 2005, Ap&SS, 296, 221
Thiemann, H. B., Norton, A. J., Dickinson, H. J., McMaster, A., & Kolb, U. C. 2021, MNRAS, 502, 1299
Tylenda, R., Hajduk, M., Kamiński, T., et al. 2011, A&A, 528, A114
van Hamme, W. 1993, AJ, 106, 2096
Vilhu, O. 1983, HiA, 6, 643
Wadhwa, S. S., De Horta, A., Filipović, M. D., et al. 2021, MNRAS, 501, 229
Wadhwa, S. S., De Horta, A. Y., Filipović, M. D., et al. 2022, JApA, 43, 94
Wadhwa, S. S., Y DeHorta, A., Filipović, M., & Tothill, N. F. H. 2023, AN, 344, e20220066
Wilson, R. E. 1990, ApJ, 356, 613
Yildiz, M., & Doğan, T. 2013, MNRAS, 430, 2029
Zhang, X.-D., & Qian, S.-B. 2020, MNRAS, 497, 3493
Zhou, X., Qian, S., Boonrucksar, S., et al. 2018, PASJ, 70, 87